K07

Proceedings of the 5th International Conference on Inverse Problems in Engineering: Theory and Practice, Cambridge, UK, 11-15th July 2005

COMPARISON OF TWO FUNCTIONALS FOR DIFFERENT MEASUREMENT PRINCIPLES FOR NON-LINEAR CAPACITANCE TOMOGRAPHY

B. KORTSCHAK and B. BRANDSTÄTTER
Christian Doppler Laboratory for Automotive Measurement Research, located at the Institute of Electrical Measurement and Measurement Signal Processing, Kopernikusgasse 24, A-8010 Graz, Austria
e-mail: kortschak@emt.tugraz.at, brand@ieee.org

Abstract – A model based, non-linear reconstruction for Electrical Capacitance Tomography (ECT) is considered as an inverse problem to find the spatial distributed permittivities in a pipe. In practice measurements are performed with a limited number of electrodes and multiple independent measurements are necessary to get information about the whole interior. In this paper the superposition of field problems is utilized to reduce to computational burden. Further two functionals are examined, which are different with respect to the underlying measurement principle. One is based on a voltage measurement and the other is based on the displacement current. These functionals are validated by two different reconstruction algorithms with data of an ECT prototype sensor.

1. INTRODUCTION

In this paper the application of two non-linear reconstruction methods for ECT is discussed. For this purpose an electrostatic representation of the field problem is appropriate, which is described by a Laplace equation. For the forward problem let ϵ denote the permittivity value of a medium, u the potential, u_0 a Dirichlet boundary condition of the exciting electrodes with the boundary Γ_0 and consider the Laplace equation

$$\begin{aligned} \nabla \cdot (\epsilon \nabla u) &= 0 && (1) \\ u\Big|_{\Gamma_0} &= u_0. && (2) \end{aligned}$$

Commonly the reconstruction can be considered as an optimization problem for identifying the permittivities from measurements in the not necessarily connected region of observation with indicator function χ ($\chi = 1$ in the region of the electrodes and $\chi = 0$ else where). In [1] ECT is performed on the assumption of a voltage measurement u_m by minimizing the following functional

$$I(\epsilon) = \int_\Omega |u(\epsilon) - u_m|^2 \, \chi \, dx + \alpha^2 R(\epsilon). \tag{3}$$

The last term in equation (3) describes a regularization, which usually is a smoothness assumption on the solution. This term depends on the reconstruction algorithm and is discussed in detail in the next section. In practice the data u_m are observed by a set of independent measurements. For a prototype sensor developed by our group (a sketch of the cross-section is shown in figure 1) two electrodes are excited by a certain voltage, whereas the other 14 electrodes act as floating electrodes. A set of measurements is obtained by switching the active electrodes according to a predefined pattern. During the minimization of the cost functional (3) an efficient calculation of the forward problems is necessary and in this paper the superposition principle is utilized to speed up the reconstruction. Thus the number of measurements can be increased to improve accuracy.

Another possibility to obtain measurements for ECT is based on displacement currents on grounded electrodes. The hardware realization of this measurement principle gives advantages with respect to in system calibration. Another point is that it is possible to compensate stray capacitances. A detailed discussion of the two measurement principles can be found in [12]. The displacement currents in the model are equivalent to electric displacements d_m on the surface of the electrodes Γ_e. For the reconstruction following functional can be considered

$$J(\epsilon) = \int_{\Gamma_e} \left| \epsilon \frac{\partial u}{\partial n} + d_m \right|^2 ds + \alpha^2 R(\epsilon) \tag{4}$$

where the forward problems satisfy the Dirichlet conditions

$$\begin{aligned} u\Big|_{\Gamma_0} &= u_0 \\ u\Big|_{\Gamma_e} &= 0. \end{aligned} \tag{5}$$

This paper is structured as follows. First two methods to tackle the forward problems are summarized. One is based on a finite element method (FEM) with a fixed grid. The second one is based on the boundary element

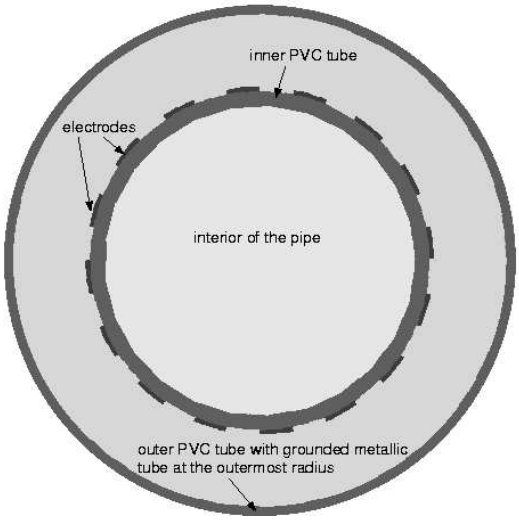

Figure 1: Cross section of the ECT sensor.

method (BEM) and a levelset formulation with an iteratively moving interface. In the next two sections the minimization of (3) and (4) is performed. Next reconstruction results with real world data of the ECT sensor are presented and the different algorithms are compared with respect to reconstruction quality. At last the conclusion gives a short outlook of future research and the appendix summarizes the material derivatives of the two functionals.

2. THE CONSIDERED FORWARD PROBLEMS AND REGULARIZATION TERMS

One possibility to tackle the inverse problem is based on a finite element approach. For a detailed description of the method the interested reader is referred to [1]. Figure 2 shows the discretization of the pipe with a fixed grid of triangles. The solution of the forward problem is calculated by the FEM. The floating electrodes are modeled as regions with high permittivity ($\epsilon_r = 10^4$). Each finite element in the interior of the pipe has a constant and unknown relative permittivity and the values are summarized into vector $\vec{\epsilon}_r$. The regularization term, which incorporates a smoothness assumption, is expressed by a discrete differential operator $\mathbf{L}$.

$$R_1(\vec{\epsilon}_r) = |\mathbf{L}\vec{\epsilon}_r|^2 \tag{6}$$

The regularization parameter α^2 is adaptively adjusted as described in [11]. For the least squares structure of the cost functionals (3) and (4) the Gauss-Newton method [4] is an efficient way to calculate the minimum of these optimization problems. The material sensitivity required for gradient based methods is calculated by the adjoint variable method and is discussed in the appendix for both cost functionals.

The second reconstruction algorithm assumes object boundaries in the interior of the pipe. Therefore it is assumed that ϵ is piecewise constant. A detailed discussion of this method can be found in [7]. The algorithm is different to the former one, which performs best for material mixtures with smooth transitions without interfaces. Figure 3 shows the discretization of the sensor with the BEM. In the interior an example illustrates an unknown

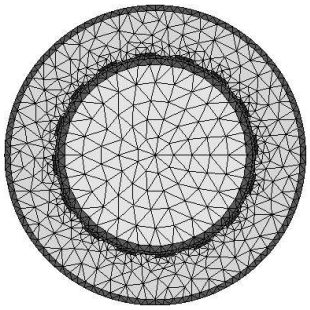

Figure 2: Discretization into triangles.

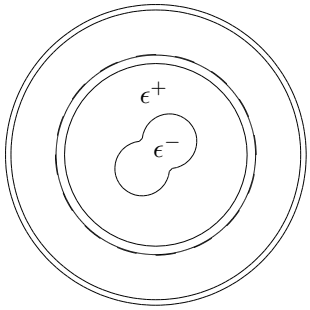

Figure 3: Discretization with boundary elements.

object boundary. The representation of the shape and its evolution during an iterative reconstruction is achieved by the level set method [9]. With this formulation the topology of a disturbance can change easily and any arbitrary shape can occur. Additionally the material properties are unknown as well. The iterative reconstruction is performed again with a Gauss-Newton algorithm to achieve fast convergence. For the regularization term different ideas are lent from image processing. For instance total variational regularization [3] or the Mumford Shah functional [10] have been used already in electrical impedance tomography. In this paper the following regularization is used (the permittivities outside and inside the interface are ϵ^+ and ϵ^-, respectively, all unknown permittivities are summarized into $\vec{\epsilon}_r$).

$$R_2(\vec{\epsilon}_r, \Gamma) = (\epsilon^+ - \epsilon^-)^2 \int_\Gamma ds \tag{7}$$

With this regularization term unrealistic high jumps in the material value are penalized (note that the magnitude of a jump can be controlled by α^2) as well as large circumferences of the interfaces .

3. RECONSTRUCTION WITH VOLTAGE DATA

As mentioned above the measurements are performed with a set of active electrodes. Table 1 shows for instance a pattern of 8 independent measurements. Two electrodes are excited by a certain voltage whereas the other 14 electrodes are floating.
The corresponding forward problems with p being the index for the active electrodes read as follows:

$$\nabla \cdot (\epsilon \nabla u_p) = 0 \tag{8}$$

$$u_p\big|_{\Gamma_{0,p}} = u_{0,p} \tag{9}$$

The Dirichlet condition $u_{0,p}$ for the active electrode p is applied on the boundary $\Gamma_{0,p}$. The spatial discretization of the functional (3) yields

$$\hat{I}(\vec{\epsilon}_r, \Gamma) = |\vec{V}(\vec{\epsilon}_r, \Gamma) - \vec{V}_m|_2^2 + \alpha^2 \cdot R(\vec{\epsilon}_r, \Gamma). \tag{10}$$

The observed voltages for the different electrode patterns and the calculated voltages are combined into $\vec{V}_m$ and $\vec{V}(\vec{\epsilon}_r, \Gamma)$, respectively. For the regularization term (6) or (7) depending on the FEM or BEM based reconstruction is used.

Additionally to the forward problems, adjoint problems have to be solved to calculate shape and material derivatives of the floating potentials ([5, 6] for fixed material properties or [2] for fixed geometry, [8] for the BEM). To summarize the results the following equation gives the derivative with respect to shape and material (the index p is omitted).

$$\frac{d}{dt} \int_{\Omega_t} u_t \, \chi \, dx \bigg|_{t=0} = \int_\Omega \epsilon' \nabla u \cdot \nabla \overline{u} \, dx + \int_\Gamma (\epsilon^+ - \epsilon^-) [\nabla u]^+ \cdot [\nabla \overline{u}]^- F_n \, ds \tag{11}$$

Ω_t is an image of Ω, which is obtained by $\vec{x}_t = \vec{x} + t\vec{F}$. The optimization steps are discrete snapshots in the artificial time t. The symbol $'$ indicates the change of the material values for a fixed geometry. The second term corresponds to the shape differentiation of an unknown interface Γ in direction F_n normal to the interface. The permittivities ϵ^+ and ϵ^- are the outer and inner permittivity, respectively. The term $[\nabla u]^+$ corresponds to the electric field in the outer region and $[\nabla \overline{u}]^-$ to the electric field of the adjoint problem in the inner region. The adjoint problem is defined as follows

$$\nabla \cdot (\epsilon \nabla \overline{u}) = \chi \tag{12}$$

$$\overline{u}\big|_{\Gamma_0} = 0, \tag{13}$$

where a charge for the measurement electrode and a homogeneous boundary condition on the transmitting electrode is applied. These adjoint problems have to be solved additionally to the forward problems.

For the solution of the partial differential equations (8) and (12) different Dirichlet boundary conditions have to be applied for each field problem. This yields different system matrices if the problems are discretized for example with the FEM or BEM. However, the prototype sensor consists of only 16 electrodes and the superposition

Table 1: Pattern of independent measurement

	electrode number							
active electrode a	1	5	3	7	2	4	6	8
active electrode b	9	13	11	15	10	12	14	16

principle, which can be applied under the assumption that the permittivities do not depend on the electric field strength, can be utilized. This means that a potential distribution can be expressed by a sum of independent potential fields. For example for 16 field problems, denoted by $u_1, u_i \dots u_{16}$, the electrode i is exited by the negative unit charge -1. Then for a specific electrode pattern p a vector $\vec{\gamma}$ with the elements γ_i exists such that

$$u_p = \sum_{i=1}^{16} \gamma_i u_i. \tag{14}$$

The resulting charges on the electrodes for this pattern are

$$\vec{Q}_p = -\mathbf{E}\vec{\gamma} \tag{15}$$

with $\mathbf{E}$ being the identity matrix. For one measurement a set of electrodes has Dirichlet boundary conditions and the other electrodes have homogeneous Neumann boundary conditions. They are floating and, due to their almost perfectly conductive surface, the total charge is zero. Hence $\vec{\gamma}$ is well defined and independent of the number of measurements an overall number of only 16 field problems have to be solved.

4. RECONSTRUCTION WITH DISPLACEMENT CURRENT DATA

The electric displacement d_m can not be measured directly. The corresponding quantity is the charge on the measurement electrodes. In the discrete model this charge is defined by the flux integrating method

$$Q_i = -\int_{\Gamma_e} \epsilon \frac{\partial u}{\partial n} ds. \tag{16}$$

Like above the charges can be summarized in vectors $\vec{Q}_m$ and $\vec{Q}(\vec{\epsilon}_r, \Gamma)$ for the measurement values and the calculated ones. This leads to following discretization of the functional (4)

$$\hat{J}(\vec{\epsilon}_r, \Gamma) = |-\vec{Q}(\vec{\epsilon}_r, \Gamma) + \vec{Q}_m|_2^2 + \alpha^2 \cdot R(\vec{\epsilon}_r, \Gamma). \tag{17}$$

The charges can be integrated easily with the BEM and for the FEM a fast charge calculation is described in [13]. The differentiation with respect to material properties and a moving interface can be solved with the adjoint variable method similar to the equation (11).

$$-Q_{i,t}|_{t=0} = \int_\Omega \epsilon' \nabla u \cdot \nabla \overline{u}\, dx + \int_\Gamma (\epsilon_+ - \epsilon_-)[\nabla u]^+ \cdot [\nabla \overline{u}]^- F_n\, ds \tag{18}$$

In this case the adjoint problems are defined as follows.

$$\begin{aligned} \nabla(\epsilon \nabla \overline{u}) &= 0 \\ \overline{u}\big|_{\Gamma_0} &= 0 \\ \overline{u}\big|_{\Gamma_e} &= 1 \end{aligned} \tag{19}$$

Thus the adjoint problems have boundary conditions on all electrodes like the forward problems. The application of superposition is very natural for this functional. Hence the overall number of field problems, which have to be solved, is equal to the number of electrodes like above.

5. COMPARISON OF RECONSTRUCTION RESULTS

Actually the prototype sensor is based on the voltage measurement principle. However with a simple modification the charge based functional can be used for the reconstruction as well. Because of the almost perfectly conducting material of the floating measurement electrodes the total charge on these is zero. Therefore the exciting voltages and the measured voltages can be applied as Dirichlet boundary conditions in the model and the current based functional can be used. The objective function minimizes the absolute value of the charge on the floating electrodes and the reconstruction converges to the true permittivity distribution.

For the first experiment reconstruction results for the different cost functionals are compared. Figure 4 shows the prototype sensor with three PVC rods inside the PVC tube. In figure 5 the reconstructions are performed with the FEM for both cost functionals. For this test 56 electrode combinations are used and the interior of the pipe is discretized with 280 finite elements (degrees of freedom). After 6 iterations the three rods can be identified in both plots even if the resulting image is blurred due to the special choice of the regularization term. Differences between the plots are caused by a different influence of the regularization term on both functionals (the range of values of

the objective function varies between the two functionals). Next figure 6 compares the reconstruction results of the combined BEM and levelset method. The unknown interface is discretized into 150 boundary elements. The initial geometry is a centered circle and the geometry as well as the material values change in the iterative reconstruction. In both images three regions are reconstructed after 20 iterations. Both functionals yield similar results.

Next the influence of the number of independent measurements is shown in figures 7a-c. The first 2, 4, and 8 electrode combinations of table 1 are used. The three images show increasing image quality and they emphasize the influence of the number of independent measurements.

6. CONCLUSION

Two non-linear reconstruction algorithms were presented briefly. For both methods two functionals were applied, which are based on different measurement principles. The optimization process uses an analytically derived gradient and it was shown that with the utilization of the superposition principle the calculations can be performed with few additional computation time. This is of importance if a non-linear reconstruction method is used for online monitoring. Additionally, the number of measurements has only a small influence on the computational burden. At last the algorithms were verified with real world measurement data and the results of both functionals show images of comparable quality.

Future work at our Institute will focus on the reconstruction with charge measurements because of the advantages in the hardware realization. Another topic is the reconstruction in three dimensions to determine accurate volume fractions. Unfortunately, the complexity and computational effort increases significantly and a fast solver for the forward problem is required.

APPENDIX

We compare the material derivative for both functionals. We start with the weak formulation of an electrostatic field

$$\int_\Omega \epsilon \nabla u \cdot \nabla \overline{u}\, dx = \int_\Gamma \overline{u} (\epsilon \frac{\partial u}{\partial n})\, ds \tag{20}$$

with the following boundary condition

$$u\Big|_\Gamma = u_0.$$

For the functional (4) a different additional boundary condition exists on the measurement electrodes. In this case Γ is divided into the parts Γ_0 and Γ_e.

$$\begin{aligned} u\Big|_{\Gamma_0} &= u_0 \\ u\Big|_{\Gamma_e} &= 0 \end{aligned}$$

Next, differentiation of equation (20) and of the boundary conditions leads to (the partial derivatives in time are denoted with $'$)

$$\int_\Omega \epsilon' \nabla u \cdot \nabla \overline{u}\, dx + \int_\Omega \epsilon \nabla u' \cdot \nabla \overline{u}\, dx = \int_\Gamma \overline{u} (\epsilon \frac{\partial u}{\partial n})'\, ds$$

$$u'\Big|_\Gamma = 0$$

and using the theorem of Green to

$$\int_\Omega \epsilon' \nabla u \cdot \nabla \overline{u}\, dx = \int_\Omega u' \nabla \cdot (\epsilon \nabla \overline{u})\, dx + \int_\Gamma \overline{u} (\epsilon \frac{\partial u}{\partial n})'\, ds.$$

Finally we compare the derivative of the potential and of the charge on the electrodes. For both cases different adjoint problems are defined:

$$\begin{aligned} \nabla \cdot (\epsilon \nabla \overline{u}) &= \chi \\ \overline{u}\Big|_\Gamma &= 0 \end{aligned}$$

$$V' = \int_\Omega u' \chi\, ds = \int_\Omega \epsilon' \nabla u \cdot \nabla \overline{u}\, dx$$

for the functional (3).

$$\begin{aligned} \nabla \cdot (\epsilon \nabla \overline{u}) &= 0 \\ \overline{u}\Big|_{\Gamma_0} &= 0 \\ \overline{u}\Big|_{\Gamma_e} &= 1 \end{aligned}$$

$$-Q' = \int_{\Gamma_z} (\epsilon \frac{\partial u}{\partial n})'\, ds = \int_\Omega \epsilon' \nabla u \cdot \nabla \overline{u}\, dx$$

for the functional (4).

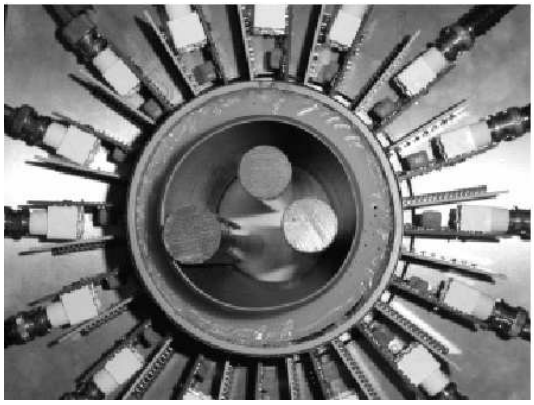

Figure 4: Prototype sensor with three PVC rods.

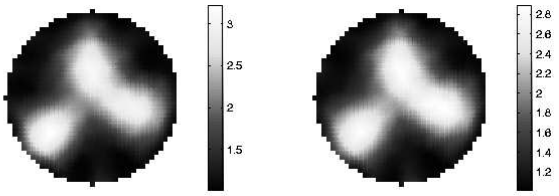

(a) Voltage based functional eq. (10).

(b) Charge based functional eq. (17).

Figure 5: Reconstruction results based on the FEM.

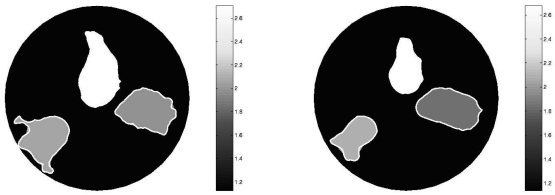

(a) Voltage based functional eq. (10).

(b) Charge based functional eq. (17).

Figure 6: Reconstruction results based on the BEM and level set formulation.

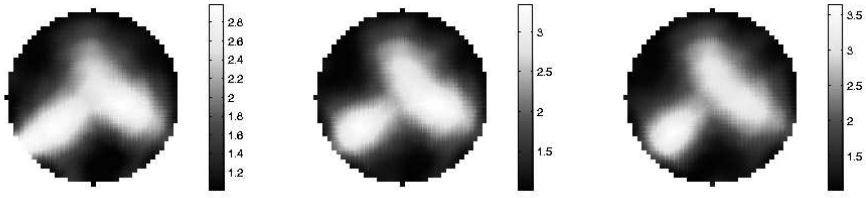

(a) 2 electrode pattern.

(b) 4 electrode pattern.

(c) 8 electrode pattern.

Figure 7: Image quality compared for different numbers of independent measurements.

REFERENCES

1. B. Brandstätter, G. Holler and D. Watzenig, Reconstruction of inhomogeneities in fluids by means of capacitance tomography. *International Journal for Computation and Mathematics in Electrical Engineering (COMPEL)* (2003), Vol.**22**(3), 508–519.

2. J. Byun, J. Lee, I. Park, H. Lee, K. Choi and S. Hahn, Inverse problem application of topology optimization method with mutual energy concept and design sensitivity. *IEEE Transactions on Magnetics* (2000), Vol.**36**, 1144–1147.

3. E.T. Chung, T.F. Chan and X.-C. Tai, Electrical impedance tomography using level set representation and total variational regularization, *UCLA Computational and Applied Mathematics Reports*, 2003.

4. R. Fletcher, *Practical Methods of Optimization*, 2nd edition, Wiley, 2000.

5. K. Ito, Level set methods for variational problems and application. *Control and Estimation of Distributed Parameter Systems* (2002), Vol.**143**, 203–217.

6. K. Ito, K. Kunisch and Z. Li, Level–Set function approach to an inverse interface problem. *Inverse Problems* (2001), Vol.**17**(5), 1225–1242.

7. B. Kortschak and B. Brandstätter, A FEM–BEM approach using level-sets in electrical capacitance tomography. Accepted for *International Journal for Computation and Mathematics in Electrical Engineering (COMPEL)* (2005), Vol.**24**(2).

8. R.A. Meric, Differential and integral sensitivity formulations and shape optimization by BEM. *Engineering Analysis with Boundary Elements* (1995), Vol.**15**, 181–188.

9. S. Osher and J.A. Sethian, Fronts propagating with curvature-dependent speed: Algorithms based on Hamilton–Jacobi formulations. *Journal of Computational Physics*. (1988), Vol.**79**, 12–49.

10. L. Rondi and F. Santosa, Enhanced electrical impedance tomography via the Mumford-Shah functional. *ESAIM: Control, Optimisation and Calculus of Variations* (2001), Vol.**6**, 517–538.

11. D. Watzenig, B. Brandstätter and G. Holler, Adaptive regularization parameter adjustment for reconstruction problems. *IEEE Transactions on Magnetics* (2004), Vol.**40**(2), 1116–1119.

12. H. Wegleiter, A. Fuchs, G. Holler and B. Kortschak, Analysis of Hardware Concepts for Electrical Capacitance Tomography Applications. submitted to *IEEE Conference on Sensors*, Irvine, California, 2005.

13. H. Yan, F.Q. Shao and S. Wang, Fast calculation of sensitivity distributions in capacitance tomography sensors. *IEE Electronics Letters* (1998), Vol.**34**(20), 1936–1937.